metals

Article

Solid-State Recycling of AA6063 Aluminum Chips via Accumulative Roll Bonding: A Green Pathway to High-Performance Materials

Mauro Carta [1,*], Noomane Ben Khalifa [2,3], Pasquale Buonadonna [1], Francesco Aymerich [1] and Mohamad El Mehtedi [1]

[1] Department of Mechanical, Chemical and Materials Engineering, University of Cagliari, 09123 Cagliari, Italy; pasquale.buonadonna@unica.it (P.B.); francesco.aymerich@unica.it (F.A.); m.elmehtedi@unica.it (M.E.M.)
[2] Institute for Production Technology and Systems, Leuphana Universität Lüneburg, 21335 Lüneburg, Germany; noomane.ben_khalifa@leuphana.de
[3] Institute of Material and Process Design, Helmholtz-Zentrum Hereon, 21502 Geesthacht, Germany
* Correspondence: mauro.carta94@unica.it

Abstract

Accumulative Roll Bonding (ARB) is a severe plastic deformation process typically used to produce ultra-fine-grained structures. This study investigates the feasibility of using the ARB process to recycle aluminum chips from an Al-Mg-Si alloy (AA6063). The chips were first compacted under a 200 kN hydraulic press and then directly hot-rolled at 550 °C without prior heat treatment to a final sheet thickness of 1.5 mm. Subsequent ARB cycles were then applied to achieve full consolidation. Mechanical properties were evaluated through tensile testing and microhardness measurements, while microstructure was characterized using Optical Microscopy and SEM-EBSD. These analyses revealed significant grain refinement and improved homogeneity with increasing ARB cycles. Mechanical testing showed that the ARB process substantially enhanced both tensile strength and hardness of the recycled AA6063 chips while maintaining good ductility. The best results were obtained after two ARB cycles, yielding an ultimate tensile strength (UTS) of 170 MPa and an elongation at rupture of 15.7%. The study conclusively demonstrates that the ARB process represents a viable and effective method for recycling aluminum chips. This approach not only significantly improves mechanical properties and microstructural characteristics but also offers environmental benefits by eliminating the energy-intensive melting stage.

Keywords: solid-state recycling; hot rolling; accumulative roll bonding; aluminum; chips; AA6063; EBSD; SEM; sustainable aluminum recycling

Academic Editor: Laszlo J. Kecskes

Received: 2 August 2025
Revised: 9 September 2025
Accepted: 17 September 2025
Published: 19 September 2025

Citation: Carta, M.; Ben Khalifa, N.; Buonadonna, P.; Aymerich, F.; El Mehtedi, M. Solid-State Recycling of AA6063 Aluminum Chips via Accumulative Roll Bonding: A Green Pathway to High-Performance Materials. *Metals* **2025**, *15*, 1042. https://doi.org/10.3390/met15091042

1. Introduction

Aluminum is a key material known for its excellent properties, such as corrosion resistance and a high strength-to-weight ratio, making it widely used in structural applications across various industrial sectors. It is the third most abundant element in the Earth's crust and is primarily produced from bauxite through an energy-intensive electrochemical process [1,2]. However, as sustainability becomes an increasingly critical global concern, aluminum recycling is emerging as an important and growing trend worldwide [3]. In fact, aluminum can be considered as a highly sustainable material, with approximately 75% of all aluminum ever produced still in use today [4]. This remarkable longevity is largely due to efficient recycling practices, which offer significant environmental benefits.

In particular, recycling aluminum requires only about 5% of the energy needed for primary production from raw materials, resulting in substantial reductions in both energy consumption and greenhouse gas emissions [5]. As a result, aluminum plays a key role in sustainable manufacturing across diverse sectors, including transportation, aerospace, construction, and packaging.

Despite these advantages, conventional recycling methods—primarily based on remelting and casting—pose some technical limitations. The remelting process leads to oxidation and the formation of dross, particularly in scrap with a high surface to volume ratio like chips [6]. Recycled alloys also tend to accumulate impurities (e.g., iron and silicon) that form brittle intermetallic compounds, reducing ductility, fracture toughness, and fatigue life. As a consequence, recycled aluminum is often "down-cycled" into lower-grade applications where performance requirements are less stringent or diluted with "pure" aluminum from primary production [3].

Solid-state recycling (SSR) techniques provide an alternative approach that eliminates melting and its associated drawbacks, leading to a lower energy consumption and material savings [7]. Among these SSR methods, several have been developed for recycling machining chips, including direct extrusion [8,9], equal channel angular pressing (ECAP) [10], friction extrusion [11,12], forging [13], and direct rolling [14]. Direct rolling has been studied only in recent years as a promising technique for the sustainable production of metal sheets. In this process, compacted chips are heat-treated and then directly subjected to hot and cold rolling through multiple passes [15] even with the usage of an envelope [16]. However, although some studies have demonstrated the potential to achieve a fine dispersion of oxides in extrusion processes with high extrusion ratios, it remains challenging to attain high levels of deformation using conventional rolling techniques [17]. An increase in strain during the process could significantly enhance the bonding between chips, as previously demonstrated in other solid-state recycling processes [18,19]. Thus, in the context of rolling, employing the Accumulative Roll Bonding (ARB) process presents a viable strategy to amplify strain, which may enhance the overall mechanical properties. Originally developed as a severe plastic deformation (SPD) technique for producing ultrafine-grain metals, the ARB process consists of repeated cycles of sheet stacking, surface preparation, and roll bonding. Each cycle introduces high plastic strain, resulting in grain refinement, enhanced bonding, and improved mechanical properties [20]. Unlike other SPD methods, ARB can be performed using conventional rolling equipment and is potentially scalable for sheet production, making it particularly attractive for industrial applications. In recent years, ARB has been successfully applied to various aluminum alloys, including both heat-treatable and non-heat-treatable series, as well as similar and dissimilar material combinations [21,22].

While previous work by the authors has demonstrated the feasibility of the direct rolling process for recycling AA6063 chips [15], including its effectiveness in reducing environmental impact [23], the present study investigates the application of Accumulative Roll Bonding (ARB) to AA6063 chips. While most prior studies on ARB have focused on bulk aluminum sheets, where the process is used mainly as a severe plastic deformation technique to refine grains and enhance strength, this research aims to develop a sustainable solid-state recycling process for producing high-performance aluminum sheets directly from machining waste (chips). This work studies microstructure evolution, mechanical behavior, and process feasibility, with particular focus on comparing different ARB cycles and evaluating their effects on bonding quality, grain refinement, and mechanical properties enhancement. This research demonstrates how ARB can upcycle aluminum machining waste into structural-grade sheet material, offering both technical and sustainability advantages that align with circular economy principles in materials manufacturing.

2. Materials and Methods

The aluminum chips used in this study were produced through dry milling (without lubricants) to avoid contamination. The chips had mean dimensions of 1.1 mm in width and 25 ± 20 mm in length. The starting material was an AA6063 alloy billet in the annealed condition supplied by Hydro Spa (Norsk Hydro, Oslo, Norway). The nominal chemical composition is provided in Table 1. AA6063 was selected due to its extensive industrial applications and the large quantities of machining waste generated during processing. The as-received material exhibited an ultimate tensile strength (UTS) of 186 MPa and an elongation at rupture of 22%.

Table 1. Chemical composition of the alloy (wt.%).

Element	Si	Fe	Cu	Mn	Mg	Cr	Ni	Zn	Ti	Al
wt.%	0.585	0.231	0.027	0.030	0.489	0.007	0.007	0.033	0.018	Bal.

For processing, 35 g of chips were compacted under an applied load of 200 kN for 1 min, (corresponding to a compacting pressure of about 110 MPa) producing billets with dimensions of 30 × 60 × 10.5 mm^3 and a relative density of approximately 68%. The chips billets were then hot-rolled in air at 550 °C, in accordance with the rolling schedule in Table 2, without any prior heat treatment, achieving a final thickness of 1.5 mm (Figures 1 and 2). Specimens were preheated in a muffle furnace from room temperature in air atmosphere, and the time from furnace exit to rolling was about 2 s. After each pass, the samples were returned to the furnace for 10 min to restore temperature. A two-high BW200 rolling mill (Carl Wezel, Mühlacker, Germany) with 130 mm rolls and a fixed rotational speed of 52 rpm was used for processing. No lubricants were used. The process is schematically shown in Figure 1.

Table 2. Rolling schedule of the compacted chips. The rolling passes are performed in temperature (hot rolling) until the 7th pass. h_x indicates the thickness after the "x-th" rolling pass. After the 7th pass, three ARB cycles were performed with a 50% thickness reduction per cycle.

Number of Passes	h0	h1	h2	h3	h4	h5	h6	h7	ARB1	ARB2	ARB3
Chips [mm]	10.5	6.5	4.4	3.2	2.4	2.0	1.8	1.5	1.5	1.5	1.5
True Strain per pass	-	0.480	0.390	0.318	0.288	0.182	0.105	0.182	0.693	0.693	0.693
Cumulative strain	-	0.480	0.870	1.188	1.476	1.658	1.764	1.946	2.639	3.332	4.025

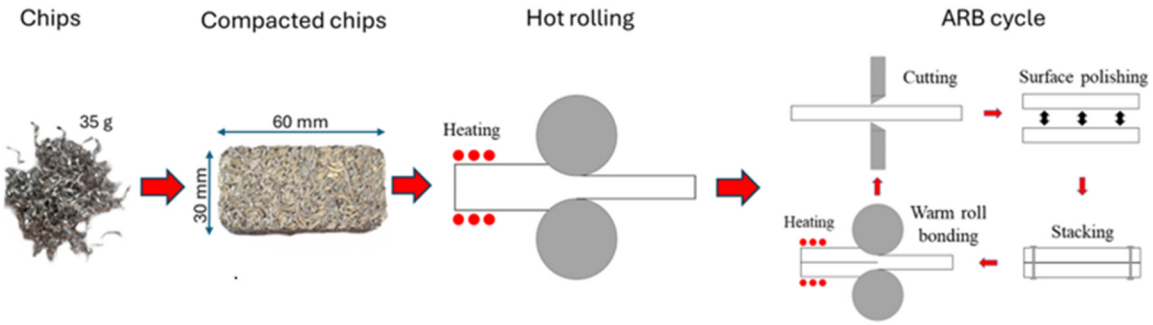

Figure 1. Schematic representation of the ARB recycling process applied to the AA6063 chips Adapted from Ref. [24].

The samples then underwent the Accumulative Roll Bonding process using the following preparation sequence (illustrated in Figure 1): each sample was cut in half lengths;

the contact surfaces were ground with 80-grit sandpaper and degreased using acetone to remove contaminants. The two parts were then stacked and mechanically joined with rivets. This preparation produced roll-bondable chips-based samples in their as-rolled condition. Prior to each ARB cycle, samples were pre-heated to 450 °C (10 min holding time) in a muffle furnace and then hot rolled with a 50% thickness reduction, to re-attain the target thickness of 1.5 mm. The complete ARB procedure was repeated for three cycles. The nomenclature ARB1, ARB2, and ARB3 refers to samples processed through one, two, and three ARB cycles, respectively.

Figure 2. Chips-based as-rolled sheet before ARB process.

Figure 3 shows the ARB-processed samples. Edge trimming of the lateral border became necessary between the ARB2 and ARB3 stages to mitigate crack formation and propagation.

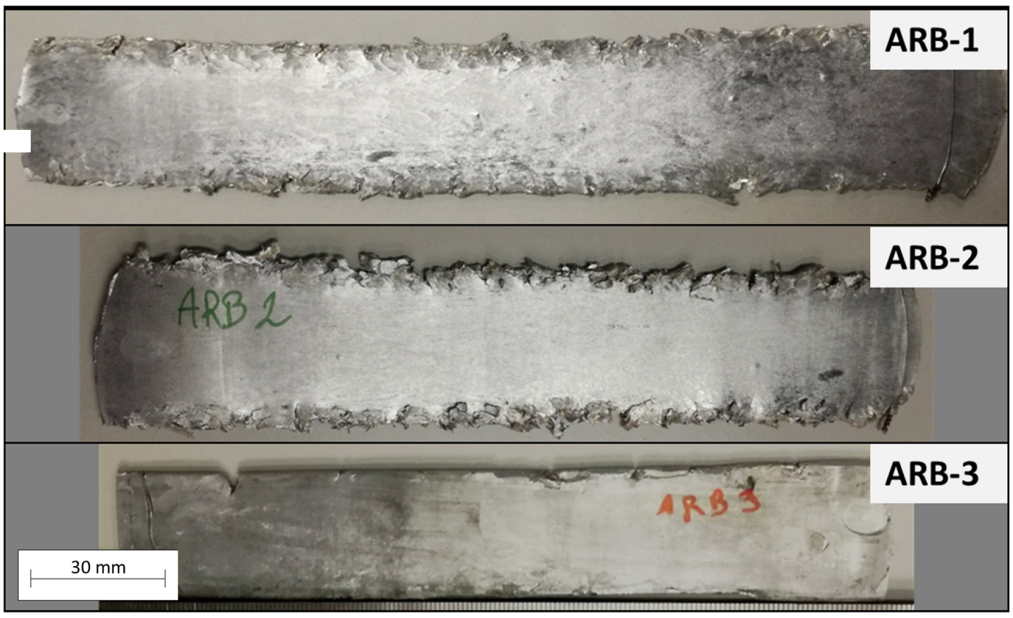

Figure 3. Macroscopic appearance of sheets following various ARB cycles.

The mechanical properties were evaluated in the as-rolled condition along the rolling direction (RD) through tensile testing and Vickers microhardness measurements.

Tensile specimens (Figure 4) were prepared according to ASTM E8/E8M and BS EN 895 standards [25,26]. Tests were conducted using a Galdabini® SUN500 universal (Cardano al Campo, Italy) testing machine, with three replicates per condition to ensure statistical reliability. Vickers microhardness measurements were taken across the thickness direction using a Shimadzu Microhardness Tester (Type M) under a 0.2 kgf load.

Microstructural evolution was characterized by using both optical microscopy and SEM/EBSD techniques. Samples for optical microscopy were sectioned along the rolling direction (RD), electropolished in 70% phosphoric acid at 75 °C, and etched with Barker's reagent (5% HBF_4). Samples were observed under polarized light using a Leica Z8 Wild

M420 optical microscope (Leica Microsystems, Amsterdam, The Netherlands). For SEM and EBSD analysis, samples were cut along the rolling direction and mechanically polished. For EBSD, samples were additionally electropolished to remove deformation layers and surface scratches using a Struers Lectropol-5 system (Struers, Ballerup, Denmark) with AC2 electrolyte, applying 20 V for 20 s.

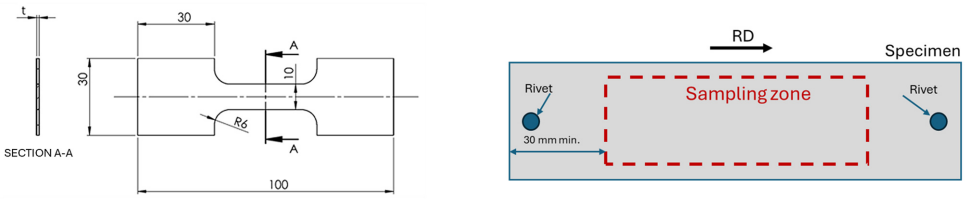

(**a**) (**b**)

Figure 4. (**a**) Tensile sample scheme and dimensions (all dimensions in mm), reprinted from Ref. [15]; (**b**) schematic illustration of the ARB stack specimen, showing rivet placement and the central region selected for tensile and microstructure sampling.

EBSD mapping was conducted on a Zeiss Ultra 55 Gemini FEG-SEM (Carl Zeiss, Oberkochen, Germany), with a scanned area of 250 × 300 μm^2 and a step size of 0.4 μm. This configuration enabled high-resolution analysis of grain structure and crystallographic orientation. All the raw EBSD data were post-processed using standard cleanup routines (Grain CI Standardization, Neighbor Orientation Correlation and Dilation operations) to improve indexing quality and grain boundary definition.

3. Results and Discussion

3.1. Microstructures

Figure 5 illustrates the microstructural evolution of recycled metal chips subjected to rolling and Accumulative Roll Bonding (ARB). All micrographs were captured under polarized light after electropolishing and Barker's etching.

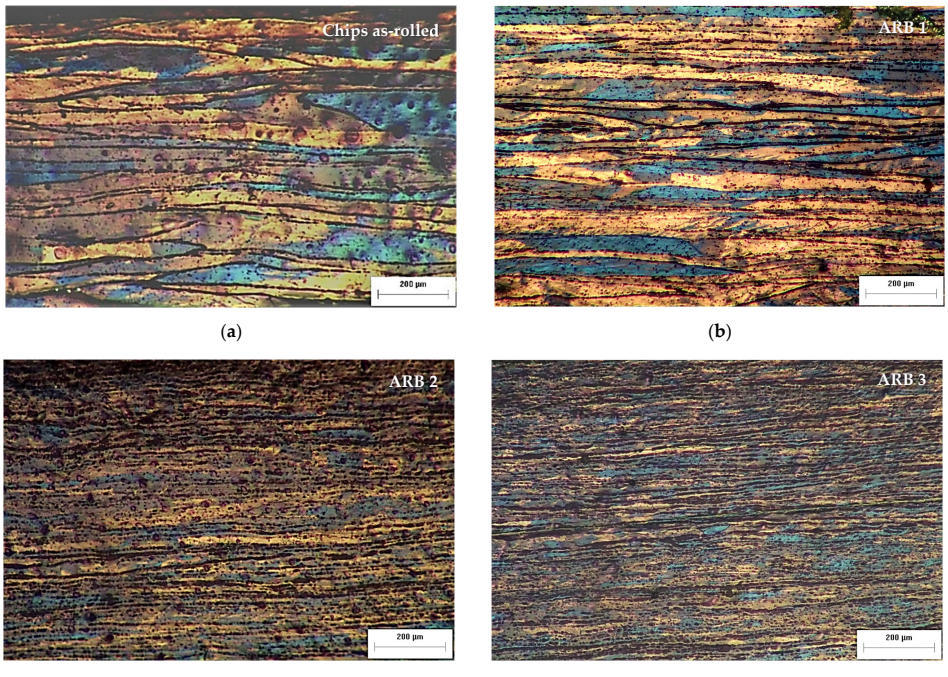

(**a**) (**b**)

(**c**) (**d**)

Figure 5. OM micrographs in the RD of (**a**) as-rolled chips before ARB process; (**b**) ARB-1; (**c**) ARB-2; (**d**) ARB-3.

In the as-rolled condition (Figure 5a), a pronounced lamellar structure is evident, characterized by elongated, poorly bonded chip interfaces. The grain structure predominantly follows the original chip boundaries, which remain distinctly visible. After the first ARB cycle (Figure 5b), partial grain refinement and increased microstructural homogeneity are observed, though the elongated grain morphology persists. By the second ARB cycle (Figure 5c), the microstructure becomes more uniform, with reduced chip boundary visibility and improved deformation consistency. After three cycles (Figure 5d), the material develops a highly refined structure, exhibiting diminished anisotropy and clearer evidence of microstructural homogenization, consistent with the severe plastic deformation (total true strain of 2.1) induced by ARB processing.

Electron Backscatter Diffraction (EBSD) measurements are showed in Figure 6. The IPF maps (Figure 6a–c) demonstrate the progressive microstructural evolution resulting from increased plastic deformation through successive ARB cycles. The corresponding grain boundary misorientation angle distributions for each condition are shown in Figure 6d–f while Figure 6g–i show the grain dimensions distribution.

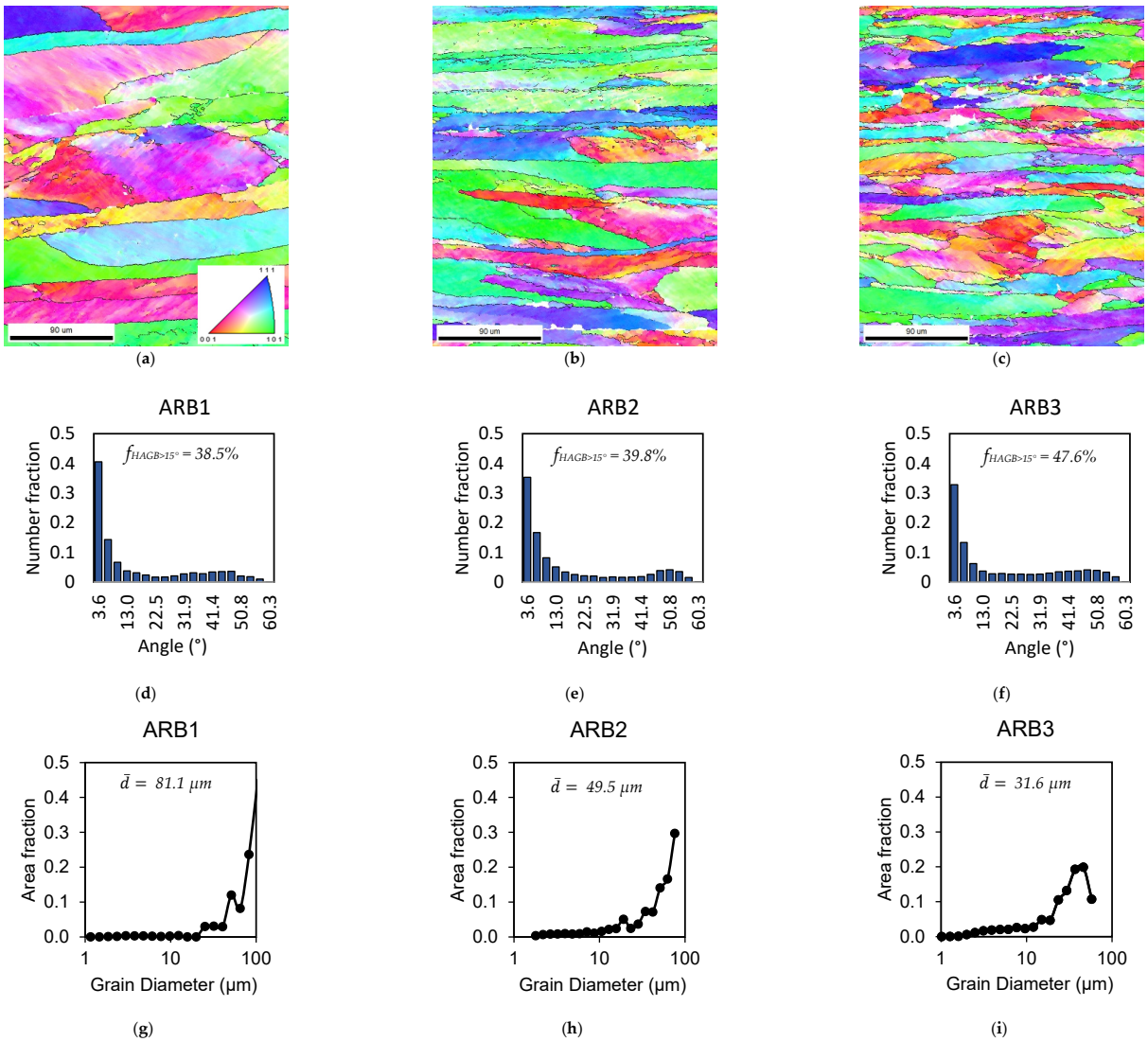

Figure 6. EBSD Analysis on ARB-ed samples. RD is aligned with the scale bars. IPF map of (**a**) ARB1, (**b**) ARB2, (**c**) ARB3, and histograms of boundary misorientation angle of (**d**) ARB1, (**e**) ARB2 and (**f**) ARB3. Grain size distributions expressed as area fraction versus grain diameter (logarithmic scale) for AA6063 chips consolidated by 1 (**g**), 2 (**h**) and 3 (**i**) ARB cycles.

In the ARB1 condition (Figure 6a), the microstructure is dominated by large, elongated grains with non-uniform orientations and a substantial presence of retained chip boundaries. These characteristics demonstrate that despite the 50% thickness reduction, the first ARB cycle produces limited plastic deformation and bonding, with chips largely maintaining their original morphology and showing minimal dynamic recovery or recrystallization. This is reflected in the grain size distribution (Figure 6g), where the mean grain diameter remains high ($\overline{d}$ = 81.1 µm), confirming the persistence of coarse grains and incomplete refinement. After two ARB cycles (Figure 6b), a more refined and fragmented microstructure becomes evident. The elongated grains appear shorter and narrower, as a result of the accumulation of strain and progressive breakup of the initial chip structure. The alignment of grains along the RD becomes more consistent, and grain boundaries are more continuous, indicating improved bonding between chips. The corresponding grain size distribution (Figure 6h) shifts toward smaller diameters, with a reduced mean grain size of $\overline{d}$ = 49.5 µm, while the misorientation histogram (Figure 6e) shows a slightly increased fraction of high-angle grain boundaries (HAGBs, >15°; 39.8%).While local dynamic recovery processes are likely active at this stage, complete recrystallization has not yet occurred. Following three ARB cycles (Figure 6c), the microstructure undergoes significant refinement, with grains displaying a more homogeneous size distribution and strong alignment along the RD. The original chip boundaries become progressively indistinct, demonstrating effective metallurgical bonding and substantial grain refinement due to severe plastic deformation. The mean grain size further decreases to $\overline{d}$ = 31.6 µm (Figure 6i), while the fraction of HAGBs rises to 47.6% (Figure 6f). This indicates that dynamic recrystallization is now the dominant mechanism, involving grain boundary migration and the formation of new, strain-free grains. The progressive increase in HAGBs and simultaneous decrease in mean grain size confirm the microstructural homogenization and refinement typical of high-strain processing routes such as ARB process, where accumulated dislocation density promotes subgrain formation and subsequent recrystallization [27]. The misorientation angle distributions reported in Figure 6d–f, provide further insights into the grain boundary evolution across ARB cycles. In the ARB1 condition (Figure 6d), the distribution is dominated by low-angle grain boundaries (LAGBs, <15°), which are typically associated with dislocation substructures formed during plastic deformation. This suggests that the first ARB cycle primarily induces strain hardening with limited recovery or recrystallization. In the ARB2 sample (Figure 6e), the histogram shows a broader distribution, with a slightly increased fraction of high-angle grain boundaries (HAGBs, >15°). But it is by the third ARB cycle (Figure 6f), that the fraction of HAGBs increases further, suggesting that dynamic recrystallization becomes more dominant. The presence of HAGBs is a strong indicator of grain boundary migration and the formation of new, strain-free grains. This transformation from LAGBs to HAGBs reflects the progressive microstructural homogenization and grain refinement induced by severe plastic deformation. These observations are consistent with previous studies on ARB-processed aluminum alloys, which report a gradual transition from dislocation cell structures to refined ultrafine grains with increasing ARB cycles [28]. The increase in HAGBs is also associated with improved mechanical properties, particularly enhanced strength coupled with preserved ductility, in accordance with the Hall–Petch strengthening relationship.

3.2. SEM and EDS Analysis

Figure 7 shows EDS elemental mapping of the ARB1 sample at 3000× magnification, displaying the spatial distribution of principal alloying elements (Si, Mg, Fe, Mn, Al, and O) in correlation with the corresponding SEM micrograph. The elemental analysis

reveals distinctive microstructural features characteristic of chips-based recycled aluminum processed by Accumulative Roll Bonding.

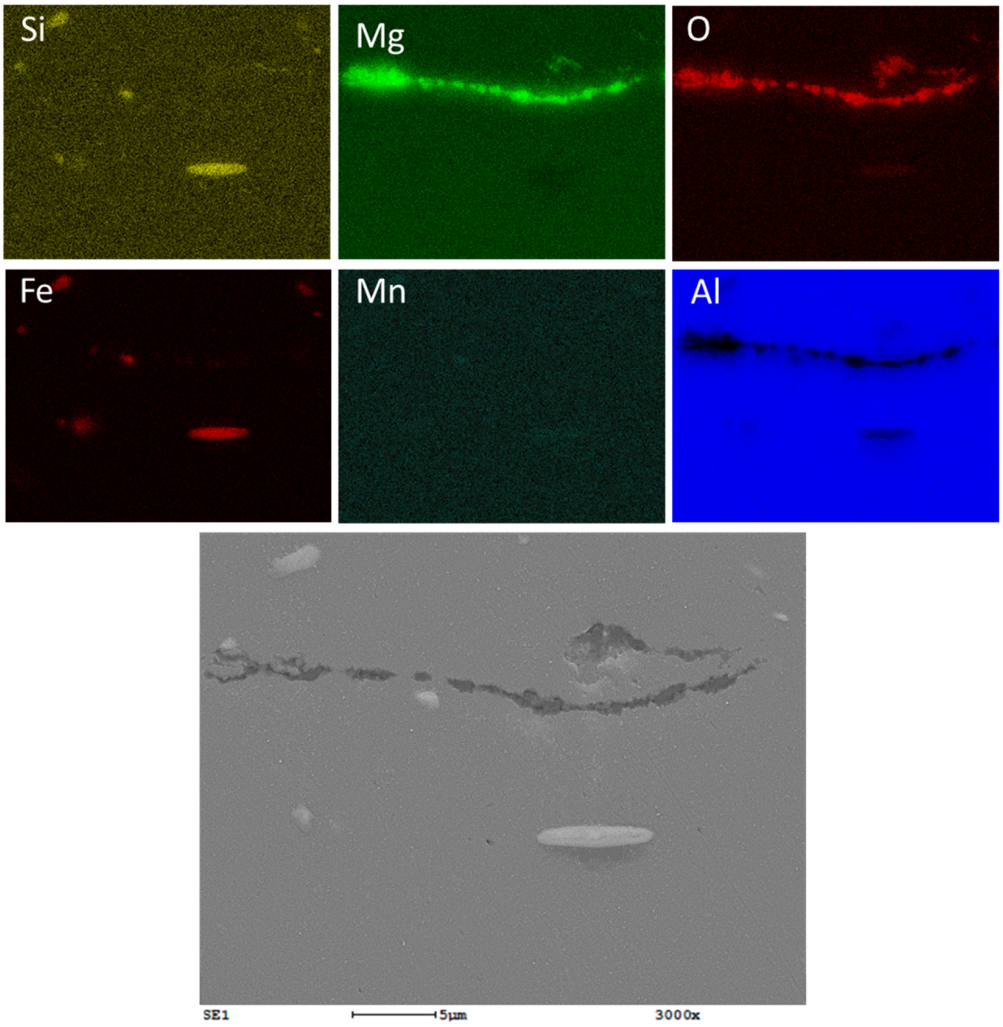

Figure 7. EDS map of an ARB1 sample, 3000×. RD aligned with the scale bar.

The bright silicon (Si) and iron (Fe) rich regions in the maps correspond to intermetallic particles, likely β-AlFeSi type, which form during solidification or thermomechanical processing of AA6xxx alloys. These intermetallics appear as light-gray phases in the SEM micrograph and are typically hard and brittle, potentially acting as crack initiation sites under mechanical stress. Their mixed morphology—elongated or rounded—and distribution confirm they are retained from the initial chips and not entirely dissolved during the ARB process. In comparison, the Mn distribution appears generally homogeneous with localized round-shaped enrichments suggesting the presence of α-Al(MnFe)Si intermetallics. This phase is typically more benign than β-AlFeSi, and its formation is promoted by Mn additions, as also reported in prior studies [29,30].

A key observation from the Mg and O elemental maps is the co-localization of magnesium and oxygen, forming continuous band-like features aligned with the rolling direction (RD). While EDS mapping cannot unambiguously distinguish between MgO, Al_2O_3, or mixed oxides, the observed chemistry strongly suggests the presence of Al/Mg-rich oxides located at prior chip boundaries (PCBs). These oxide networks are a well-known feature of solid-state recycled aluminum, often originating during machining when the high surface-to-volume ratio of chips promotes rapid oxidation [31,32]. Other authors [33] have reported that, in SSR of chips of 6xxx alloys, a ~10 nm native Al_2O_3 layer forms,

while MgO islands initially grow up to ~60 nm until reaching a surface coverage of ~90%, after which they thicken further. Excessive oxide formation can be mitigated by restricting the exposure time of chips to high temperatures in air. In the SEM micrograph, PCBs appear as darker, irregular paths distinct from the surrounding matrix. With increasing strain in subsequent ARB cycles, these oxide networks tend to fragment and redistribute. Importantly, their alignment along RD confirms they deform together with the aluminum matrix. Such oxide accumulations at interfaces can reduce bonding quality and locally deplete Mg from the matrix, thereby potentially hindering Mg_2Si precipitation and limiting strengthening potential. The persistence of these oxides in ARB1 explains the inferior bonding quality and reduced ductility observed during mechanical testing and fracture surface analysis. Additionally, these oxygen-rich zones serve as obstacles to dislocation motion and stress transmission, generating weak points unless adequately fragmented and dispersed in subsequent processing stages.

Figure 8 presents EDS map of ARB3 sample of recycled chips of AA6063 aluminum alloy. When compared to the ARB1 sample (Figure 7), the ARB3 microstructure shows clear evidence of refinement and redistribution of interfacial phases, indicating significant microstructural evolution due to the increased plastic deformation imposed by three ARB cycles.

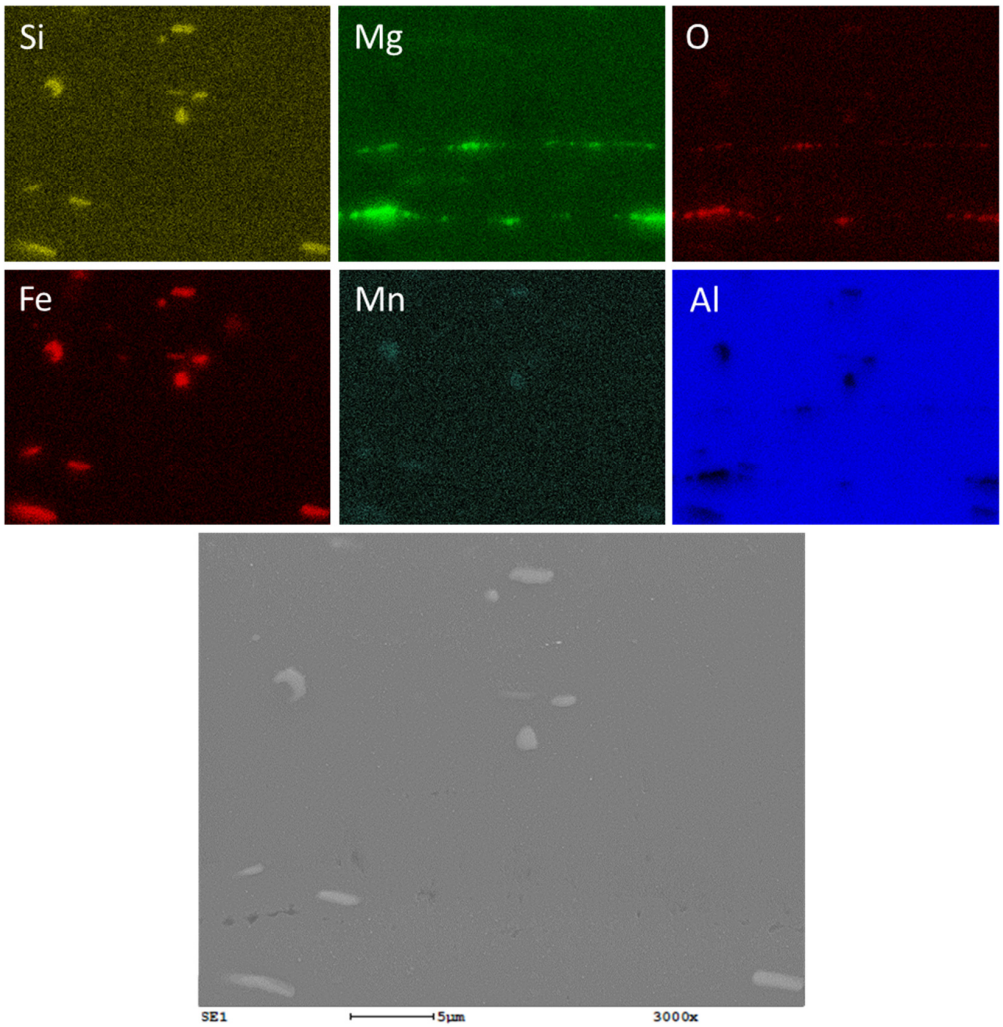

Figure 8. EDS map of an ARB3 sample, 3000×. RD aligned with the scale bar.

The Mg and O maps in Figure 8 still reveal the presence of Mg and O-rich bands, but these appear more fragmented and thinner than in the ARB1 condition. The Mg-and

O-rich features are still present, but they appear thinner and more discontinuous than in ARB1, suggesting progressive fragmentation of prior chip boundary oxides under severe plastic deformation. Their increased discontinuity reflects improved inter-chip bonding and enhanced matrix continuity. The Al map further confirms this homogenization, showing a more uniform distribution with fewer signs of local depletion near oxide boundaries. The observed microstructural evolution implies a higher degree of consolidation and matrix continuity, consistent with the enhanced mechanical properties and ductile fracture behavior of ARB3 samples. In the Si and Fe maps, again β-AlFeSi intermetallics appear as discrete bright spots corresponding to light-gray regions in the SEM micrograph. These are more finely dispersed and less clustered than in ARB1, indicating fragmentation or redistribution during processing. Importantly, the Mn map, although still weak, shows a slightly enhanced intensity near Fe-Si rich areas, indicating partial transformation of β-phase intermetallics to α-Al(MnFe)Si phases, a phenomenon favored under thermomechanical processing conditions.

Table 1 (Figure 7) and ARB3 (Figure 8) clearly demonstrates how accumulated strain disrupts oxide networks and refines intermetallic particles. The ARB1 condition shows continuous MgO/Al_2O_3 films and unbroken PCBs, which act as weak interfaces that compromise mechanical performance. In contrast, ARB3 exhibits fragmented and discontinuous oxide networks and homogenously distributed intermetallics, consistent with the grain refinement and improved boundary misorientation characteristics revealed by EBSD analysis (Figure 6c).

3.3. Mechanical Properties

Figures 9 and 10 show the mechanical properties of AA6063 recycled chips after undergoing different cycles of Accumulative Roll Bonding (ARB), while Table 3 summarized the mechanical properties of AA6063 recycled by accumulative roll bonding (ARB) compared with typical values for wrought AA6063 in O, T4, and T6 tempers.

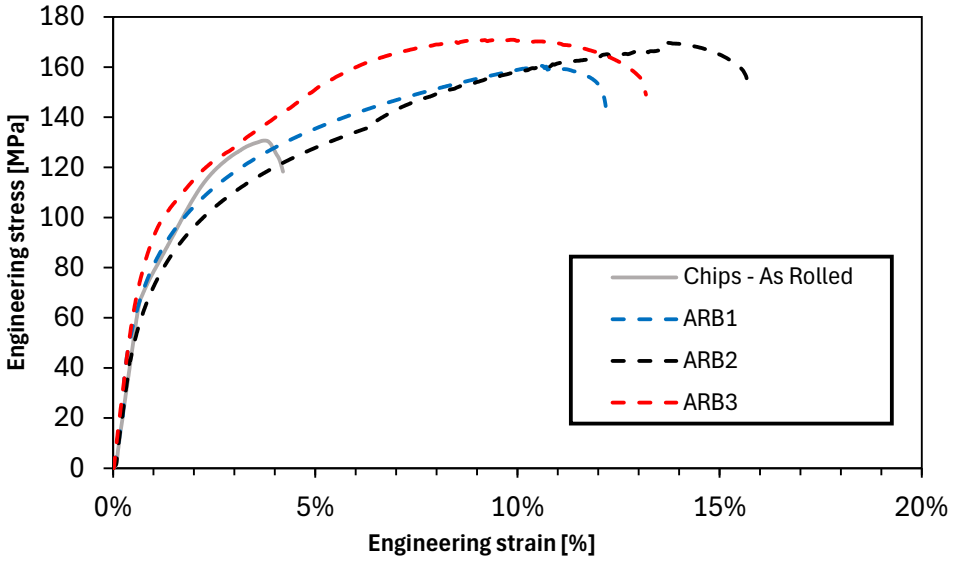

Figure 9. Representative stress–strain curves of all the tested samples in as-rolled condition and along the RD.

The black line in Figure 10a represents the Ultimate Tensile Strength (UTS) across all the studied conditions. It shows a consistent upward trend across the ARB cycles, indicating an improvement in material strength through processing. The UTS starts at 131 MPa in the as-rolled chip condition (before ARB process), increases to 161 MPa at

ARB1, continues rising to 170 MPa at ARB2, and reaches 171 MPa at ARB3. The red line in Figure 10a represents the elongation at break (A%). Ductility improves markedly from the chips as-rolled condition (4.2%), rising to 12.2% at ARB1 and peaking at 15.7% at ARB2. However, it slightly decreases to 13.2% at ARB3, though it remains significantly higher than the starting condition.

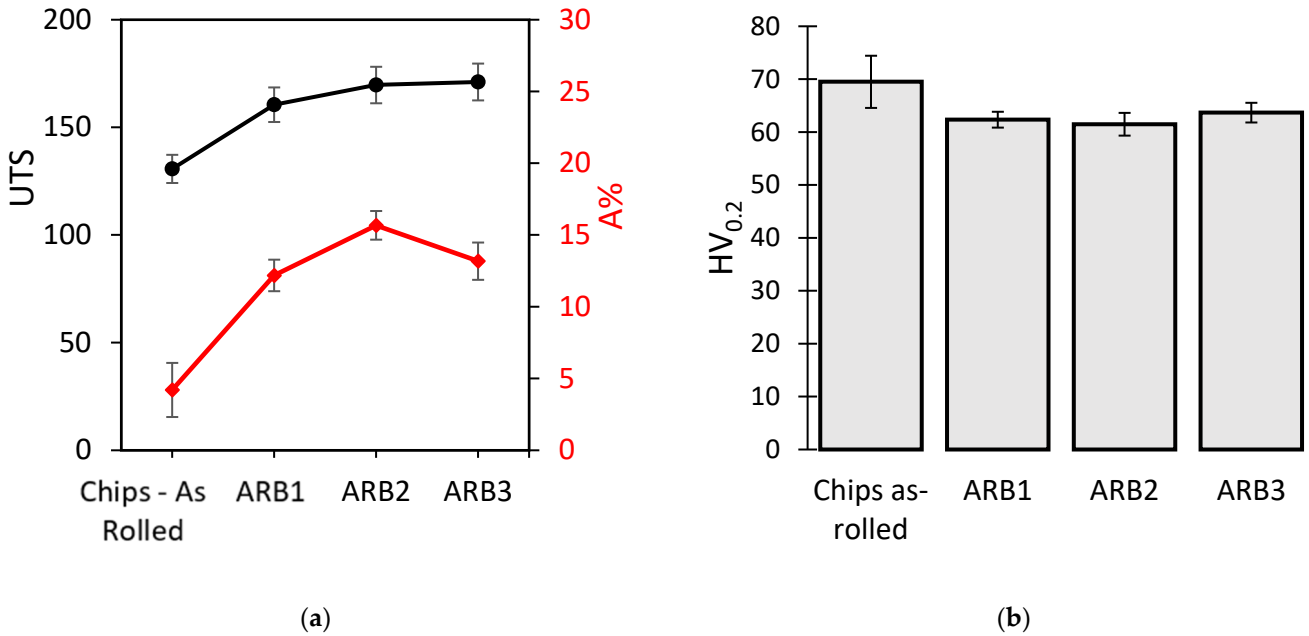

(**a**) (**b**)

Figure 10. Mechanical properties of pre-ARB and ARBed samples: (**a**) UTS and elongation at break; (**b**) Vickers microhardness (with 0.2 Kgf applied load).

Table 3. Mechanical properties of AA6063 recycled by accumulative roll bonding (ARB), compared with typical values for wrought AA6063 in O, T4, and T6 tempers.

	Chips As-Rolled	ARB 1	ARB 2	ARB 3	Typical AA6063 Wrought Alloy (O) [34]	Typical AA6063 Wrought Alloy (T4) [34]	Typical AA6063 Wrought Alloy (T6) [34]
Proof Stress [MPa]	75 ± 4	69 ± 3	62 ± 5	83 ± 4	50	90	215
UTS [MPa]	131 ± 7	161 ± 8	170 ± 9	171 ± 9	90	170	240
A% [%]	4.2 ± 1.9	12.2 ± 1.1	15.7 ± 1.0	13.2 ± 1.3	-	22	12

Figure 10b shows the Vickers microhardness ($HV_{0.2}$) of the material. The hardness is relatively stable across all ARB-ed samples, with a very slight upward trend, implying that with successive ARB cycles, the change in hardness is not as pronounced as the changes in tensile strength and ductility. In the as-rolled condition, the chips exhibit higher hardness. However, as the number of ARB cycles increases, the AA6063 recycled chips tend to become stronger but with a peak of ductility after 2 ARB cycles, with minimal changes in microhardness.

The mechanical response of ARB-processed AA6063 chips shows a distinct behavior compared to both bulk ARB material and the standard T6 condition [35]. While ARB applied to bulk AA6063 increases yield strength (up to 236 MPa), it significantly reduces elongation (from 20% to 6.8%). In contrast, chips subjected to ARB exhibit a simultaneous increase in strength and ductility: UTS rises from 131 MPa to 171 MPa, and elongation improves from 4.2% to 15.7% at ARB2. Notably, this ductility exceeds that of the T6 condition (12%), despite lower UTS. These results highlight the effectiveness of solid-state recycling

via ARB in enhancing both sustainability and mechanical performance. The mechanical properties of AA6063 significantly improve with an increasing number of ARB cycles, as also confirmed by other results reported in the literature [36]. However, this comes at the cost of reduced ductility, dropping from 25 to 30% in the annealed state to 11–13% after ARB. This decline is attributed by the authors to increased strain hardening and reduced dislocation mobility. Interestingly, at higher cycles, improved microstructural homogeneity and refined shear texture promote better strain distribution, partially recovering ductility and enhancing plastic anisotropy. Moreover, as shown by Jafarian et al. [37], ARB-treated AA6063 alloys can achieve exceptional low-temperature superplasticity, with elongations up to 270% at 300 °C. This confirms that the ultrafine grain structures induced by ARB facilitate both strength and formability, offering promising perspectives for sustainable, high-performance aluminum recycling.

3.4. Fracture Surfaces

Figure 11 shows the SEM fracture surfaces of the AA6063 recycled samples after (a) 0 cycle, (b) 1 cycle, (c) 2 cycles, and (d) 3 cycles of Accumulative Roll Bonding process. SEM micrograph of the as-rolled AA6063 chips show insufficient metallurgical bonding and the presence of interfacial cracks. The other three samples display a ductile fracture mechanism, characterized by the presence of dimples formed by microvoid coalescence. However, the morphology and distribution of these dimples evolve significantly with the number of ARB cycles, reflecting the microstructural changes observed in the EBSD analysis (Figure 6).

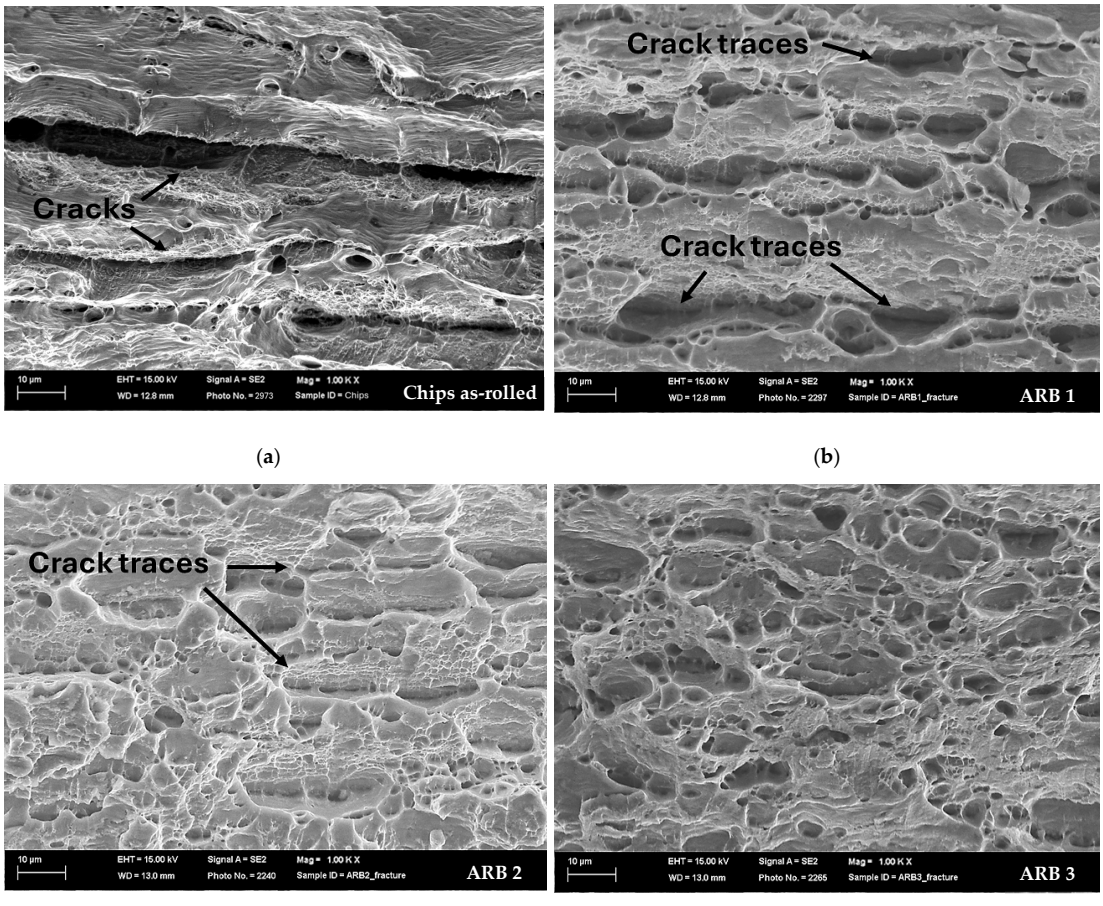

Figure 11. Fracture surfaces of ARB-ed samples, after (**a**) 0 cycle, (**b**) 1 cycle, (**c**) 2 cycles and (**d**) 3 ARB cycles. 1000× magnification.

The as-rolled condition (a) reveals insufficient metallurgical bonding, with visible interfacial cracks and unbonded chip boundaries, indicative of poor consolidation during the initial rolling step. In contrast, the ARB1 sample (b) exhibits a predominantly ductile fracture characterized by dimples of heterogeneous size and scattered flat regions with crack traces. These features suggest incomplete bonding between chips and the persistence of initial interfaces or oxide layers, consistent with the EBSD map (Figure 6a), which shows coarse, elongated grains and a high fraction of low-angle grain boundaries (LAGBs). After two ARB cycles (Figure 11c), the fracture surface becomes more homogeneous, with finer and more uniformly distributed dimples. However, some crack traces from PCBs are still visible. This refinement correlates strongly with the EBSD results, which show a noticeable decrease in grain size. The slightly increased presence of HAGBs suggests the onset of dynamic recrystallization, which contributes to improved plasticity and enhanced metallurgical bonding between chips. This transition is reflected in the fracture morphology, where the dimples are more consistent in size and depth, indicating a more uniform stress distribution during tensile loading.

In the ARB3 sample (Figure 11d), the dimples become even finer and more evenly distributed across the fracture surface, indicating extensive grain refinement and the highest level of plastic deformation. The corresponding EBSD map (Figure 6c) confirms this evolution, showing a dense and uniform network of recrystallized grains with a higher fraction of HAGBs and smaller grain dimensions. This microstructural state facilitates more homogeneous deformation and energy absorption during fracture, contributing to a refined ductile surface appearance. While mechanical testing showed a slight reduction in ductility for ARB3 compared to ARB2, the fracture surface appears without crack traces and a uniform distribution of dimples.

Together, the fracture surface morphology and EBSD data demonstrate a consistent and progressive improvement in microstructural integrity with increasing ARB cycles. The evolution from irregular, interface-dominated fracture (chips as-rolled) to refined, homogeneous ductile fracture (ARB2 and ARB3) is directly linked to the microstructural transformation captured by EBSD—from elongated grains with low misorientations to a highly refined grain structure. These observations linked well with the mechanical testing results shown in Figures 9 and 10. The reduction in pit size and the more uniform distribution observed are consistent with the additional grain refinement revealed by EBSD analysis. Using chips as the starting material inevitably introduces microstructural complexities, such as residual chip boundaries and oxide films. The ARB process, through repeated deformation and consolidation, progressively fragments and disperses these heterogeneities while promoting grain refinement and microstructural homogenization. The predominance of ductile fracture features further indicates that bonding between chips is effective, allowing the recycled sheets to sustain significant plastic deformation.

The present work was carried out on clean AA6063 machining chips to demonstrate the baseline feasibility of ARB. The robustness of the process when applied to typical industrial scrap streams, which often exhibit variability in alloy origin, surface contamination, and lubricant residues, remains an open question. Such heterogeneity can affect interfacial bonding, oxide morphology, and mechanical consistency. Nevertheless, the severe plastic deformation imposed during ARB is expected to provide a certain tolerance by fragmenting and redistributing oxides and inclusions. To fully assess robustness under industrial conditions, further studies on mixed-origin and contaminated scrap streams are required, including evaluation of minimal preprocessing strategies (such as chips cleaning) needed to ensure reproducible product quality.

4. Conclusions

This study demonstrates the feasibility and benefits of using Accumulative Roll Bonding (ARB) as a solid-state recycling method for AA6063 aluminum chips. The main conclusions are as follows:

- Direct hot rolling of compacted chips without heat treatment resulted in poor bonding and suboptimal mechanical properties;
- The ARB process significantly improved chip consolidation; after two cycles, the material reached a UTS of 170 MPa and an elongation at break of 15.7%;
- Microstructural observations revealed progressive grain refinement; EBSD analysis showed an increase in high-angle grain boundaries and reduced grain elongation with each ARB cycle, indicating recrystallization and improved homogeneity;
- SEM and EDS analyses confirmed the breakup and redistribution of oxides and intermetallic phases, contributing to enhanced mechanical behavior and cleaner fracture surfaces;
- Although the ARB process is effective, it still faces industrial challenges, including manual preparation steps, the absence of lubricants, and roll sticking. However, its compatibility with conventional rolling equipment makes it a promising solution for upcycling aluminum scrap into high-performance products.

In summary, ARB enables the recovery of high-strength, ductile aluminum sheets from recycled chips without melting, offering a viable route to sustainable, closed-loop manufacturing in industries such as automotive, aerospace, and packaging.

Author Contributions: Conceptualization, M.C., M.E.M. and P.B.; methodology, M.C., N.B.K. and M.E.M.; software, M.C. and M.E.M.; validation, M.C., N.B.K. and P.B.; formal analysis, M.C. and P.B.; investigation, M.C., F.A. and P.B.; resources, M.C., N.B.K. and M.E.M.; data curation, M.C. and F.A.; writing—original draft preparation, M.C.; writing—review and editing, M.C., M.E.M., N.B.K. and P.B.; visualization, M.C.; supervision, N.B.K. and M.E.M.; project administration, N.B.K. and M.E.M.; funding acquisition, M.E.M. and M.C. All authors have read and agreed to the published version of the manuscript.

Funding: This research was funded by Ecosystem of Innovation for Next generation Sardinia (ECS00000038)—Spoke 7 (Low Carbon Technologies for efficient energy system), PNRR, Mission 4, Component 2, Investment line 1.5—by the European Union—NextGenerationEU—Project Title: "RILAMIAL—Innovative Recycling of Aluminum Alloys through Direct Rolling for a Sustainable Future"—CUP: F53C22000430001.

Data Availability Statement: The original contributions presented in this study are included in the article; further inquiries can be directed to the corresponding author/s.

Conflicts of Interest: The authors declare no conflicts of interest.

References

1. Rudnick, R.L.; Gao, S. Composition of the Continental Crust. In *Treatise on Geochemistry*; Holland, H.D., Turekian, K.K., Eds.; Elsevier-Pergamon: Oxford, UK; London, UK, 2003; Volume 3, pp. 1–64.
2. Das, S.K.; Yin, W. The worldwide aluminum economy: The current state of the industry. *JOM* **2007**, *59*, 57–63. [CrossRef]
3. Raabe, D.; Ponge, D.; Uggowitzer, P.J.; Roscher, M.; Paolantonio, M.; Liu, C.; Antrekowitsch, H.; Kozeschnik, E.; Seidmann, D.; Gault, B.; et al. Making sustainable aluminum by recycling scrap: The science of "dirty" alloys. *Prog. Mater. Sci.* **2022**, *128*, 100947. [CrossRef]
4. Al Mahmood, A.; Kader, A.; Islam, M.B.; Hossain, R. Sustainable transformation of waste Aluminium into high-performance composites: A review. *Int. J. Light. Mater. Manuf.* **2025**, *8*, 194–204. [CrossRef]
5. Al-Alimi, S.; Yusuf, N.K.; Ghaleb, A.M.; Lajis, M.A.; Shamsudin, S.; Zhou, W.; Altharan, Y.M.; Abdulwahab, H.S.; Saif, Y.; Didane, D.H.; et al. Recycling aluminium for sustainable development: A review of different processing technologies in green manufacturing. *Results Eng.* **2024**, *23*, 102566. [CrossRef]

6. Altharan, Y.M.; Shamsudin, S.; Al-Alimi, S.; Saif, Y.; Zhou, W. A review on solid-state recycling of aluminum machining chips and their morphology effect on recycled part quality. *Heliyon* **2024**, *10*, e34433. [CrossRef] [PubMed]
7. Shamsudin, S.; Lajis, M.; Zhong, Z. Solid-state recycling of light metals: A review. *Adv. Mech. Eng.* **2016**, *8*, 1687814016661921. [CrossRef]
8. Tekkaya, A.; Schikorra, M.; Becker, D.; Biermann, D.; Hammer, N.; Pantke, K. Hot profile extrusion of AA-6060 aluminum chips. *J. Mech. Work. Technol.* **2009**, *209*, 3343–3350. [CrossRef]
9. Gronostajski, J.; Marciniak, H.; Matuszak, A. New methods of aluminium and aluminium-alloy chips recycling. *J. Mech. Work. Technol.* **2000**, *106*, 34–39. [CrossRef]
10. Mani, B.; Paydar, M. Application of forward extrusion-equal channel angular pressing (FE-ECAP) in fabrication of aluminum metal matrix composites. *J. Alloys Compd.* **2010**, *492*, 116–121. [CrossRef]
11. Bocchi, S.; Zambelli, M.; D'urso, G.; Giardini, C. Efficiency and Microstructural Forecasts in Friction Stir Extrusion Compared to Traditional Hot Extrusion of AA6061. *J. Manuf. Mater. Process.* **2024**, *8*, 172. [CrossRef]
12. Baffari, D.; Buffa, G.; Campanella, D.; Fratini, L. Design of continuous Friction Stir Extrusion machines for metal chip recycling: Issues and difficulties. *Procedia Manuf.* **2018**, *15*, 280–286. [CrossRef]
13. Altharan, Y.M.; Shamsudin, S.; Al-Alimi, S.; Jubair, M.A. Development of Zirconia Reinforced AA7075/AA7050 Aluminum Chip-Based Composite Processed Using Hot Press Forging Method. *Int. J. Technol.* **2023**, *14*, 5. [CrossRef]
14. El Mehtedi, M.; Buonadonna, P.; El Mohtadi, R.; Loi, G.; Aymerich, F.; Ben Khalifa, N.; Carta, M. Feasibility Study of Solid-State Recycling through Direct Hot Rolling of AA5754 Aluminum Chips for Automotive Applications. *Mater. Sci. Forum* **2024**, *1130*, 3–12. [CrossRef]
15. Carta, M.; Ben Khalifa, N.; Buonadonna, P.; El Mohtadi, R.; Bertolino, F.; El Mehtedi, M. Innovative Solid-State Recycling of Aluminum Alloy AA6063 Chips Through Direct Hot Rolling Process. *Metals* **2024**, *14*, 1442. [CrossRef]
16. El Mehtedi, M.; Carta, M.; Buonadonna, P. A Novel Direct Hot Rolling Process for Sustainable Recycling of AA3105 Alu-minum Chips Using a Protective Envelopment. *Manuf. Lett.* **2025**, *45*, 70–74. [CrossRef]
17. Chino, Y.; Hoshika, T.; Lee, J.-S.; Mabuchi, M. Mechanical properties of AZ31 Mg alloy recycled by severe deformation. *J. Mater. Res.* **2006**, *21*, 754–760. [CrossRef]
18. Hu, M.-L.; Ji, Z.-S.; Chen, X.-Y.; Wang, Q.-D.; Ding, W.-J. Solid-state recycling of AZ91D magnesium alloy chips. *Trans. Nonferrous Met. Soc. China* **2012**, *22*, s68–s73. [CrossRef]
19. Zhang, T.; Ji, Z.; Wu, S. Effect of extrusion ratio on mechanical and corrosion properties of AZ31B alloys prepared by a solid recycling process. *Mater. Des.* **2011**, *32*, 2742–2748. [CrossRef]
20. Saito, Y.; Utsunomiya, H.; Tsuji, N.; Sakai, T. Novel ultra-high straining process for bulk materials—development of the accumulative roll-bonding (ARB) process. *Acta Mater.* **1999**, *47*, 579–583. [CrossRef]
21. El Mehtedi, M.; Lai, D.; Almehtedi, R.; Carta, M.; Buonadonna, P.; Aymerich, F. Bonding of similar AA3105 aluminum alloy by Accumulative Roll Bonding process. *ESAFORM* **2021**. [CrossRef]
22. Ghalehbandi, S.M.; Malaki, M.; Gupta, M. Accumulative Roll Bonding—A Review. *Appl. Sci.* **2019**, *9*, 3627. [CrossRef]
23. Carta, M.; Ben Khalifa, N.; Buonadonna, P.; Mele, A.; El Mehtedi, M. Life cycle assessment (LCA) of a novel solid-state recycling process for aluminum alloy AA6063 chips via direct hot rolling. *Mater. Res. Proc.* **2024**, *41*, 2881–2890. [CrossRef]
24. El Mehtedi, M.; Buonadonna, P.; Carta, M.; El Mohtadi, R.; Mele, A.; Morea, D. Sustainability Study of a New Solid-State Aluminum Chips Recycling Process: A Life Cycle Assessment Approach. *Sustainability* **2023**, *15*, 11434. [CrossRef]
25. *ASTM E8/E8M-2016a*; Test Methods for Tension Testing of Metallic Materials. ASTM International: West Conshohocken, PA, USA, 2013.
26. *UNI EN 895:1997*; Prove Distruttive sui Giunti Saldati di Materiali Metallici—Prova di Trazione sui Campioni di Grosso Spessore (Destructive Tests on Welded Joints in Metallic Materials—Transverse Tensile Test). UNI: Milan, Italy, 1997.
27. Babu, V.; Shanmugavel, B.P.; Padmanabhan, K.A. Effects of processing temperature and number of passes on the microstructure and mechanical properties of AA 6063 processed by cyclic expansion extrusion. *Arch. Civ. Mech. Eng.* **2021**, *21*, 38. [CrossRef]
28. Alvandi, H.; Farmanesh, K. Microstructural and Mechanical Properties of Nano/Ultra-fine Structured 7075 Aluminum Alloy by Accumulative Roll-Bonding Process. *Procedia Mater. Sci.* **2015**, *11*, 17–23. [CrossRef]
29. Kuijpers, N.; Vermolen, F.; Vuik, C.; Koenis, P.; Nilsen, K.; van der Zwaag, S. The dependence of the β-AlFeSi to α-Al(FeMn)Si transformation kinetics in Al–Mg–Si alloys on the alloying elements. *Mater. Sci. Eng. A* **2005**, *394*, 9–19. [CrossRef]
30. Que, Z.; Mendis, C.L. Heterogeneous nucleation and phase transformation of Fe-rich intermetallic compounds in Al–Mg–Si alloys. *J. Alloys Compd.* **2020**, *836*, 155515. [CrossRef]
31. Zhang, Z.; Liang, J.; Xia, T.; Xie, Y.; Chan, S.L.I.; Wang, J.; Zhang, D. Effects of Oxide Fragments on Microstructure and Mechanical Properties of AA6061 Aluminum Alloy Tube Fabricated by Thermomechanical Consolidation of Machining Chips. *Materials* **2023**, *16*, 1384. [CrossRef]
32. Laurent-Brocq, M.; Lilensten, L.; Pinot, C.; Schulze, A.; Duchaussoy, A.; Bourgon, J.; Leroy, E.; Tekkaya, A.E. Solid state recycling of aluminium chips: Multi-technique characterization and analysis of oxidation. *Materialia* **2023**, *31*, 101864. [CrossRef]

33. Duchateau, T.; Lilensten, L.; Zhang, X.; Gebhard, J.; Tekkaya, A.E.; Laurent-Brocq, M. Effect of annealing on oxidation during solid-state recycling of aluminium chips. *J. Alloys Compd.* **2024**, *1010*, 178178. [CrossRef]
34. *ASM Specialty Handbook: Aluminum and Aluminum Alloys*; Davis, J.R., Ed.; ASM International: Almere, The Netherlands, 1993; ISBN 978-0-87170-496-2.
35. Arigela, V.; Palukuri, N.; Singh, D.; Kolli, S.; Jayaganthan, R.; Chekhonin, P.; Scharnweber, J.; Skrotzki, W. Evolution of microstructure and mechanical properties in 2014 and 6063 similar and dissimilar aluminium alloy laminates produced by accumulative roll bonding. *J. Alloys Compd.* **2019**, *790*, 917–927. [CrossRef]
36. Jafarian, H.; Miyamoto, H. Tailoring Microstructure and Mechanical Properties of Nano/Ultrafine Grained AA6063 Alloy Processed by Accumulative Roll Bonding Process. *Iran. J. Mater. Sci. Eng.* **2020**, *17*, 1–10. [CrossRef]
37. Jafarian, H.; Anijdan, S.M.; Miyamoto, H. Observation of low temperature superplasticity in an ultrafine grained AA6063 alloy. *Mater. Sci. Eng. A* **2020**, *795*, 140015. [CrossRef]